Utrecht University

Master of Biofabrication

Graduate School Of Life Sciences

Minor Internship Report

Fabrication of Vascularized Model for Bone Marrow Engineering

Natacha Levy

Supervisor:
Dr. Riccardo Levato, PhD

Daily Supervisor:
Dr. Marisa de Oliveira Asunçao, PhD

Second examiner:
Dr. Debby Gawlitta, PhD

September 26, 2022

UMC Utrecht

Levato Lab
FROM SHAPE TO FUNCTION

Contents

Layman Summary

Within the bone, a soft, spongy tissue filled with blood vessels, called the bone marrow, is home to cells able to develop all blood cell types, also known as hematopoietic stem cells. The bone marrow creates a unique environment for these cells to carry out their important functions ranging from carrying oxygen throughout the body to playing a significant role in our immune system. Biological and physical signals within the bone marrow help maintain this environment. Diseases of the bone marrow are hard to establish since this environment is highly complex and still not fully understood even in the healthy state. The current treatment options for these diseases are invasive and can damage the tightly regulated environment of the bone marrow. Novel therapies harnessing the power of stem cells have been developed relying on bone marrow transplants however, there are still not enough appropriate donors and the product resulting from the transplants is relatively low. To establish better understanding of the disease states and thus develop better treatment options, we need deeper insight into the bone marrow environment. Currently, most of our knowledge has come from small animal models or two-dimensional models which limit our understanding since these models cannot accurately represent the human bone marrow. More advanced models have been generated in the past few years. Research has been focused on creating models that are able to represent the environment in three-dimension using bioprinting. This kind of technology can help recreate the native environment outside of the body which becomes very valuable to test drugs, novel therapies or even to increase our knowledge on the bone marrow such as the type of cells present and their function but also the interactions between these cells and their environment. The research that was conducted during this project aimed at fabricating an environment that would most closely resemble the native bone marrow using and harnessing the power of novel and cutting edge bioprinting technologies. By combining bioprinting with materials that can mimic essential components of the bone marrow it was possible to recreate crucial physical and biological properties of the bone marrow environment. The construct fabricated was then able to host cells normally present in the human bone marrow, for a short time showing some biological activity. Not only did we manage to recreate a physical environment in 3D we also investigated certain conditions that could help deepen our understanding of the environment and the cells that reside in it such as the stem cells. We investigated conditions that could be favorable to host different cell types found in the bone marrow. This project laid the foundation for future bone marrow specific projects but also for future projects using this bioprinting technique as we used specific chemical reactions that had never been used with this method.

Abstract

The bone marrow is a highly complex environment making diseases of the bone marrow such as hematological malignancies difficult to establish. Currently the majority of our understanding of these niche-specific phenomena have been obtained from small animal and two dimensional models which have a limited spatiotemporal resolution and do not always accurately reproduce the function of human bone marrow. This research aimed to biofabricate a vascularized bone marrow three-dimensional model for bone marrow engineering. We developed a gelMA hydrogel combined with a visible light crosslinking system for volumetric bioprinting which mimics the physical properties of bone marrow and supported vessel-like structure formation. Conditions for the co-culture of vascularized structures and hematopoietic stem cells were investigated and revealed that, the presence of serum in the culture medium is essential for vessel formation, macromolecular crowding promotes niche cell proliferation, niche cells are functional in hypoxic environment, and finally the negative effect of hematopoietic stem expansion medium on cellular metabolism can be mitigated by the addition of endothelial growth medium.

1 Introduction

The bone marrow and its complex microenvironment is home to the hematopoietic stem cells (HSCs), which give rise to all blood cell type lineages through hematopoiesis [1]. HSCs comprise our blood and immune system, with functions ranging from carrying oxygen throughout the body to being responsible for the daily production of immune cells [2, 3]. HSCs must be able to either lay quiescent or multiply and differentiate in response to external stimuli for the hematopoietic system to maintain homeostasis. By keeping HSCs lodged in specific niches, the bone marrow environment provides for these specific functions [4].

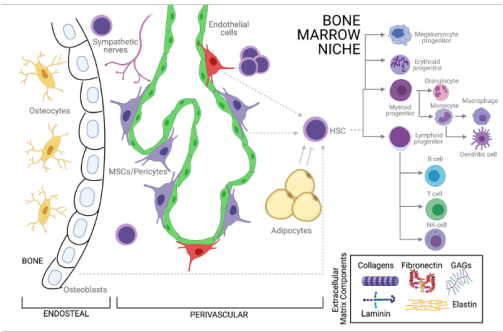

Figure 1: Key players comprising the bone marrow microenvironement in the maintenance of hematopoietic stemm cells. ©The Author(s) [5]

Two major niches can be distinguished: the perivascular niche and endosteal niche. Each niche is defined by its location and function regarding the maintenance and regulation of certain types of hematopoietic stem and progenitor cells (HSPCs) [6].The perivascular niche hosts the active and dividing HSCs and progenitor cells as well as endothelial and perivascular supporting cells [2]. Vascular endothelial cells (VEC) are one of the most prevalent niche cells in the bone marrow microenvironment due to the prominent vascularization of the bone marrow, which encompasses a large surface area [7]. The essential paracrine signaling cues required to support tissue repair and regeneration are provided by VECs, which act as passive channels providing nutrients and meeting metabolic demands that are essential for tissue repair and regeneration [7]. Following an HSC insult, a crucial phase for ensuring that the hematopoietic system returns to homeostasis is the regeneration of the structural and functional integrity of the endothelial niche [7, 8].

The quiescent HSPCs are located closer to the other niche, the endosteal niche, which comprises osteoblasts and osteoclasts on the periphery of the bone marrow[2]. Within the niche, regulatory signals come from neighboring cells in the form of bound or released molecules, as well as physical cues including oxygen tension, shear stress, contractile forces, and temperature [9]. Secreted factors mediate indirect communication between stem and niche cells. These factors have a variety of effects, including stimulating HSC expansion and releasing HSC-niche adhesion molecules.

A key component of the stem cell niche is the extracellular matrix (ECM), which supports neighboring cells and acts as an anchor for stem cells [10, 9, 11]. Protein composition of the ECM can also influence the interaction of the matrix with stem cells. ECM components are spatially maintained by specific surrounding bone marrow stromal cells including collagen I-XI, fibronectin, laminin, elastin, glycosaminoglycans (GAGs) [12]. These components are expressed differently in the different compartments of the niche. For example, collagen IV and laminin are present in the perivascular niche. Collagen I, vitronectin, periostin, osteocalcin are concentrated in the endosteal

niche while fibronectin is present throughout the niche [2]. Within the bone marrow a stiffness gradient (0.1KPa to 3KPa) from perivascular to endosteal niche reigns with the endosteal side exhibiting stiffer properties compared to the perivascular side [13]. The hydrostatic pressure from vessel to stroma also plays an important role within the niche [9]. Moreover, the hematopoietic system is characterized by a low oxygen tension (hypoxic) environment required for HSC quiescence and self-renewal [14, 15].

The bone marrow is a highly complex environment, thereby making diseases of the bone marrow such as hematological malignancies, difficult to establish [2]. Moreover, the current treatment options, which consist of mainly irradiation and chemotherapy, can cause damage to the bone marrow, limiting the regeneration and differentiation capacity of HSCs by lowering their numbers and generating functional impairments among the surviving HSCs [16, 1]. Stem cell therapy through bone marrow transplants has led to substantial clinical advances in cancer treatment [17]. However, there is still a lack of appropriate adult allogeneic donors and a poor stem cell yield from cord blood donation [9, 1]. Deeper insight into human hematopoiesis including the interaction between the various cell types is crucial for better understanding of homeostasis and disease state and thus the development of novel therapies for these diseases.

The majority of our current understanding of these niche-specific phenomena have been obtained from small animal and two dimensional (2D) models which have a limited spatiotemporal resolution and do not always accurately reproduce the function of human bone marrow [18]. More recently, the emergence of multicellular models such as organ-on-a-chip models has enabled the emulation of organ specific functions and processes in vitro. For instance, the organ-on-a-chip model of vascularized human bone marrow niches developed by [18] recreated the bone marrow perivascular and endosteal niches and showed vascularization and maintenance of HSCs. The model demonstrates the importance of a perfusable vascular network for niche maintenance and function. While these microfluidics approaches focus on communication and interaction between cell types and compartmentalization of the bone marrow, the microphysiological relevance is still low. Few three dimensional (3D) models of the bone marrow have been reported. For example, [19] recently showed the importance of a 3D model to recapitulate native structure to promote cell-cell interaction which accurately described cellular heterogeneity of multiple myeloma. However, it remains challenging to modulate the complexity and upscale these models, as well as observing how the different physiological features will affect stem cell fate.

Bioprinting technologies have made massive advances in the field of regenerative medicine. and may help overcome some of these challenges especially considering the freedom of design it offers. Current bioprinting and additive manufacturing processes all generate 3D structures layer by layer [20]. Instead, Volumetric Bioprinting (VBP) allows for the development of whole constructs at once. VBP allows for the development of entire cell-laden complexes of any size and architecture in a matter of seconds [20]. This method has shown that free-form hydrogel living tissue constructs with a complex shape can be produced without impacting cell survival [20, 21, 22]. The use of VBP could upscale the production of 3D models, and provide better representation of bone marrow as cells can interact in the 3D environment.

The aim of this project was the biofabrication of a vascularized bone marrow model for bone marrow engineering. This goal was achieved by 1) establishing VBP of hydrogel with bone marrow mimicking properties 2) establishing conditions for co-culture of vascularized structures and HSCs. We hypothesize that 1) VBP will enable the biofabrication of ECM based hydrogel with properties

tailorable to match those of the bone marrow perivascular niche and 2) conditions favorable for HSC biology will help maintain vessel like structure. A common type of hydrogel crosslinking chemistry used for light-activated 3D-bioprinting currently is a chain-growth polymerization reaction [5]. Gelatin methacryloyl (GelMa), is a well established photocrosslinkable polymer obtained from denatured collagen and has gained versatility as a bioink [23]. GelMA is a particularly interesting photocrosslinkable material as it offers excellent biocompatibility, proper degradability, has inherent biological activity and tunable physical and chemical properties [24]. These characteristics make gelMA hydrogel the ideal material for studying biological responses since it can offer attachment sites and signals that can direct cell culture and growth. GelMA hydrogel is thus a desirable candidate for replicating native ECM in cell culture [25]. As mentioned, the ECM is crucial in controlling cellular fates and has a significant impact on the regeneration and repair of damaged organs and tissues [26]. Hydrogels are created as synthetic ECMs with 3D network topologies to facilitate the exchange of nutrients and signaling chemicals and to provide microenvironments for cell adhesion, proliferation, and migration. Therefore, mimicking the ECM both biologically and physically becomes especially relevant to truly represent the bone marrow niche environment.

In order to create a customizable support material, we developed a formulation based on gelMA combined with Ruthenium and Sodium Persulfate (RuSPS) as a photoinitiator system for VBP. Ruthenium (Ru), a transition metal complex, can be coupled to sodium persulfate (SDS) to create a visible light initiating system. When irradiated with visible light, the photo-excited Ru donates electrons to SPS (Figure 2 b). After accepting electrons, SPS dissociates into sulfate anions and sulfate radicals (Figure 2 b). These radicals are subsequently able to cross-link Gel-MA by propagating through the methacryloyl groups [5]. RuSPS not only crosslinks the methacrylates in gelMA it is also able to crosslink tyrosines which is valuable for decorating the hydrogels with biological molecules that also contain tyrosines. The high bioactivity hosted in the material combined with the VBP could produce free form structures from a volume of cell-laden hydrogels in tens of seconds.

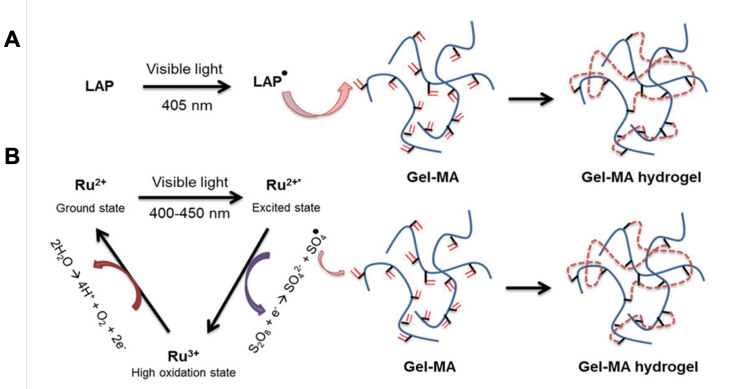

Figure 2: Gel-MA cross-linking process using A. visible light and LAP. B. visible light and RuSPS. © 2019 WILEY-VCH Verlag GmbH & Co. KGaA, Weinheim. Adapted from [5]

Finally, to establish conditions for the co-culture of vascularized structures and HSCs, we simulated several culture conditions known to be favorable for HSC biology. Modifying the culture medium used for the co-culture of ECs and mesenchymal stromal cells (MSC) revealed that the presence of serum in the medium may be essential for vessel formation, macromolecular crowding may promote proliferation of vascular niche cells and the negative effects of HSC expansion medium can be mitigated by combining the medium with commonly used EC growth basal medium. Moreover, placing

the co-culture in a low-oxygen environment showed that these vascular niche cells are functional in hypoxic environments.

2 Materials and Methods

2.1 Materials

GelMA (80% DoF) was synthesized as previously reported [27],and used as a 5%, 4% or 3% w/v% solution in phosphate-buffered saline (PBS). Lithium phenyl(2,4,6-trimethylbenzoyl)phosphinate (LAP, Tokyo Chemical Industry, Japan), tris(2,2-bipyridyl)dichlororuthenium(II) hexahydrate (Ru), Sodium Persulfate, Trypsin-EDTA solution (0.25%), Dithiothreitol (DTT) (Sigma Aldrich, Germany). Ethidium homodimer, calcein-AM (ThermoFischer, USA). CultrexTM Basement Membrane Extract (BME, R&D Systems, USA). Resazurin sodium salt (Alfa Aesar, Germany). Ficoll PM 400 density gradient media, Ficoll PM 70 density gradient media (Cytiva, Sweden). Silicone elastomer, Polydimethylsiloxane (PDMS) (Dow, The Netherlands). Eppendorf® Galaxy® 170R CO2 Incubator (New Brunswick, The Netherlands).

2.2 Fabrication of Gel-MA Hydrogels

Dried sterile Gel-MA was dissolved in PBS at 37°C. Prior to cross-linking, the Gel-MA solution was heated to 37°C. To induce a photocrosslinking reaction, either 0.1% (w/v) LAP or 0.1mM Ru and 10mM SPS were used to fabricate 5% hydrogels, 0.08mM Ru and 8mM SPS for 4% hydrogels, and 0.06mM Ru and 6mM SPS for 3% hydrogels.

2.3 Fabrication of GelNor Hydrogels

Dried sterile Gel-Nor was dissolved in PBS at 37°C. To induce a photocrosslinking reaction 0.1% (w/v) LAP and 7, 4, 2, and 1mM DTT were used to fabricate 5%, 4%, and 3% hydrogels.

2.4 Volumetric Bioprinting

Using a Tomolite printer (Readily3D, Switzerland), VBP of various structures was accomplished. MSCs were placed into 10 mm-diameter cylindrical borosilicate glass vials for bioprinting at densities ranging from 2 to 6.25×10^6 cells per mL of various gelMA bio resins. To induce thermal gelation and inhibit cell sedimentation during the printing process, the bioresin-filled vials were set at 4 °C. A laser beam at a wavelength of 405 nm was used to activate the printing process when focused on a DMD and manipulated into tomographic projections. The printing vials were then imaged with these projections. Using the software (Apparite, Readily 3D, Switzerland), the projections were computed [21]. 9.98 mW cm2 of light were emitted on average before the printing container during printing. Further literature can be found for more information about the tomographic printing process [28, 20]. Following printing, unpolymerized bioresin was melted in the printer vials by heating them to 37 °C for 30 seconds. Samples were then washed in preheated PBS. By varying the exposure period, prints at various light dosages were produced for the printing optimization tests. When all planned feature objects could be resolved and the print did not melt again after heating the bioresin, crosslinking had been successful . Finally, the printed parts underwent 5 min of additional crosslinking in 0.1% w/v LAP in PBS solution in a CL-1000 Ultraviolet Crosslinker (λ =365 nm; UVP, USA) or in 0.1mM Ru and 10mM SPS in PBS solution for 5% hydrogels, 0.08mM Ru and 8mM SPS for 4% hydrogels, and 0.06mM Ru and 6mM SPS, under floodlight (λ =450-460 nm).

2.5 Metabolic Activity

Alamar blue assay was performed to determine the metabolic activity of cells after 1, 3, 7, and 9 days (n=3). Samples were incubated in their respective culture medium containing 10% Alamar blue reagent for 4 hours. The reagent is reduced from blue to pink by metabolically active cells. The reduction in AlamarBlue reagent was calculated after measuring the absorbance ranging between 544 and 590 nm(CLARIOstar® Plus, BMG Labtechnology, Germany).

2.6 Viability Assay

Cell viability was evaluated using a live/dead assay after 1, 7, and 14 days (n = 3), imaged by a Thunder imaging system (Leica Microsystems, Germany). The samples were washed with PBS before being stained for 30 minutes with0.25 μL mL^{-1} of calcein-AM and 0.5μL mL^{-1} ethidium homodimer. Dead cell nuclei stained red, while live cells stained green. Using ImageJ software (Bio-Formats plugin), the number of live and dead cells was determined. The following equation was used to determine the cell viability:

$$Viability(\%) = (\frac{Number\ of\ live\ cells}{Number\ of\ live\ cells + Number\ of\ dead\ cells}) \times 100 \quad (1)$$

2.7 Mechanical Testing

2.7.1 Dynamical Mechanical Analysis

The stiffness of the fabricated hydrogels was measured at room temperature using a dynamic mechanical analyzer (TA instruments, DMA 2980). Unconfined compression testing was performed at ramp strain from -20% to -30% strain per minute on hydrogels samples (5 mm diameter × 2 mm thickness), with an initial static force of 0.001N was applied. Sample diameter was measured using vernier calipers, and the compressive modulus was calculated from the slope of the linear region of the stress–strain curves [29].

Physico-chemical properties
According to [30], all samples were weighed for the initial wet mass (m_{dry},t_0) after cross-linking, and three samples were lyophilized immediately to obtain their dry weights (m_{dry},t_0). These samples were then submerged in a bath of PBS and incubated at 37 °C. Samples were removed from the incubator after 1 day, blotted dry, and weighed ($m_{swollen}$). The swollen samples were then freeze-dried and weighed again (m_{dry}). The mass swelling ratio (q) was calculated as follows:

$$q = (\frac{m_{swollen}}{m_{dry}}) \quad (2)$$

2.8 Refractive Index

The refractive index of bioresins with different SPS and Ru concentrations was measured with an Abbe refractometer (2WAJ, Optika, Italy).

2.9 Microscopy and imaging

Macroscopic images of constructs printed with the volumetric bioprinter were acquired using an Olympus SZ61 stereo microscope coupled with an Olympus DP70 digital camera (Olympus Soft Imaging Solutions GmbH, The Netherlands). Fluorescence microscope (Olympus IX53) was used

for imaging of Thunder imaging systems (Leica, Germany) with 70% strength and 16900 nm feature scale. All microscope images were formatted using ImageJ [31].

2.10 Anchoring Strategy

2.10.1 Anchored GelMa constructs

Poly-di-methyl-siloxane (PDMS) molds were fabricated using Elastomer as a curing agent, with the ratio between the curing agent and the PDMS being 1:10 (weight). After thorough mixing, the solution is degassed under a vacuum pump for 30 minutes followed by 4 hours at 50°C. PDMS sheets were punctured with a 5mm puncher to cast the hydrogels or punctured with a 10mm puncher to cast the anchor around the 5mm hydrogel. Hydrogels (5% GelMA, 0.1% LAP) are casted in the 5mm molds and thermally gelated for 10 minutes at 4°C. The 5mm molds are replaced by the 10mm molds placed around the thermally gelated hydrogel. GelMA 15% (0.1% LAP) is warmed up at 37°C for a few minutes, and added around the 5mm thermally gelated hydrogels. The bottom of the petri dish is dipped into a bath of warm water until the 5% warms up and mixes with 15% gel (15 seconds). Once the two gels start to fuse, the dish is placed on ice to stop further mixing. A PDMS sheet is added on top of the mold containing the hydrogels. The gels then underwent 5 min of crosslinking in a CL-1000 Ultraviolet Crosslinker (λ=365 nm; UVP, USA).

2.10.2 Anchored Cultrex BME constructs

The anchoring process was adapted to use with cultrex instead of a gelMA 5% casted hydrogel. The petri dish was first placed at 4°C, with the 10mm punched PDMS sheet with, in its center, a 5mm PDMS disk. The 15% gelMA was distributed around the 5mm PDMS disk and placed at 4°C for 10 minutes to thermally gelate. The 5 mm PDMS disk is then removed and replaced with cultrex and placed at 37°C to allow for the cultrex to solidify (15 minutes). Once the cultrex is solidified, the undergo 5 min of crosslinking in a CL-1000 Ultraviolet Crosslinker (λ=365 nm; UVP, USA)

2.11 Cell Culture

hMSCs were cultured with alpha-Minimum Essential Medium (α-MEM, ThermoFischer,USA) supplemented with, 10% Fetal bovine serum (FBS), 1% Penicillin-Streptomycin, 1% Ascorbic acid and 0.1% FGF. Endothelial Colony Forming Cells (ECFCs) were cultured with EBM™-2 Endothelial Cell Growth Basal Medium-2 supplemented with 10% FBS, Hydrocortisone, hFGF-B, VEGF , R3-IGF-1, Ascorbic Acid, hEGF, GA-1000, Heparin (EGM2, Lonza,The Netherlands). The culture medium was replaced every 2 days and subcultured at 80 90% confluency. StemSpan™ serum-free hematopoietic cell expansion media supplemented with FBS, IL-6, FLT-3, IL-3, SCF, Primocin, TPO, Insulin, Transferrin, 2-Mercaptoethanol (StemCell Technologies, Canada). Macromolecular crowding (MMC) was introduced by dissolving Ficoll 400 (25mg/ml) and Ficoll 70 (37,5mg/ml) in EGM2 media. Hypoxia was introduced by placing the samples in a low oxygen incubator (5.0% CO2, 5.0% O2). StemSpan combination medium was made by mixing equal parts EGM2, StemSpan both supplemented individually with respective supplements including 4% FBS.

2.12 Vessel Length Quantification

The microscope images were uploaded to AngioTool (AngioTool®, [32]), which is a computational tool able to quantify vessel networks based on a set of parameters.

2.13 Statistical Analysis

Mean and standard error of the mean were used to present the results (S.E.M.). GraphPad Prism 9.0 was used for statistical analysis (GraphPad Software, USA). One or two-way ANOVAs were used to compare the experimental groups with post-hoc Sidak's multiple comparisons test. Non-parametric tests were used when normality could not be assumed. When p¡0.05, differences were considered to be significant.

3 Results

3.1 Development of Bioink for Volumetric Bioprinting of Bone Marrow Model

3.1.1 High cell density can be printed with volumetric bioprinting

We printed a 5% w/v gelMA-based bioresin supplemented with 0.1% w/v lithium phenyl-2,4,6-trimethylbenzoylphosphinate (LAP) as photoinitiator carrying a single cell suspension of a hMSCs (Figure 3) in the form of a disk (diameter= 5mm, thickness = 2mm). The bioresin was photocrosslinked at an exposure dose of 250 mJ cm^{-2} with a cell density of 6.25Million cells per ml. This light dose was used based on the work previously achieved by [21] and colleagues who printed with liver cells. Stretching of the cells within the construct can be observed.

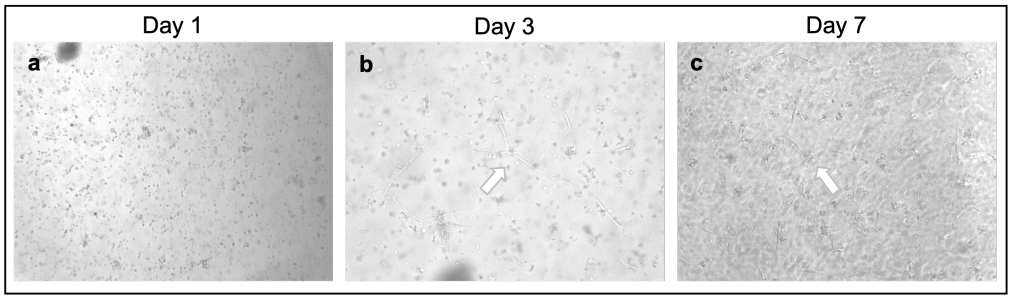

Figure 3: hMSCs encapsulated in volumetric bio printed 5% gelMA hydrogels. Constructs were monitored over 7 days. (a) Image representing the cell-laden hydrogel on the first day of culture. (b) Image representing the cell-laden hydrogel at day 3 of culture, white arrow indicates cell stretching within the construct. (c) Image representing the cell-laden hydrogel at day 7 of culture white arrows indicate cell stretching within the construct. GelMa hydrogels were crosslinked using 0.1% LAP at 250 mJ cm^{-2} printing light dose.

3.1.2 Visible Light Photoinitiating System Ruthenium Sodium Persulfate for Volumetric Bioprinting

Since RuSPS photocrosslinking system had never been reported to crosslink gelMA with VBP, optimization of the concentration of the photoinitiator and the light dose emitted was necessary. To assess the resolution of the prints, two holes of 1 mm and 2 mm diameter were implemented within the disk 3D model (5mm diameter, 2 mm thickness). In an ideal print, both features should solidify at the same time after receiving the same, optimal light dose while respecting the size of the original STL file. Exceeding this optimal dose will cause overcuring of the fine feature, and clogging of the disk. To quantify the resolution of the prints a score was established (appendix 6.1). Different concentrations of SPS were tested, 10, 15, and 20mM while keeping the Ru concentration constant at 0.1 mM. The results of this optimization process are displayed in figure 4. High concentration of SPS led to unstable prints or prints that formed only one of the holes. The light dose giving stable

prints and consistent prints that most closely resembled the original STL file was determined to be 470 mJcm^{-2}.

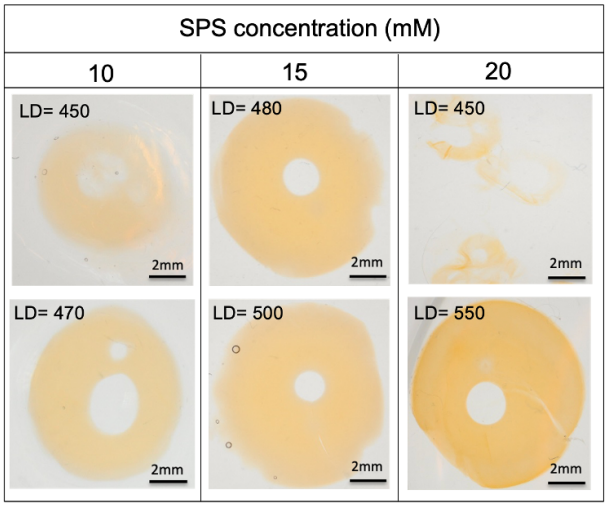

Figure 4: Different concentrations of Ru and SPS affect the resolution of prints. Stereoscope images of volumetric bioprinted gelMA hydrogels with varying Sodium Persulfate (SPS) concentration. From left to right columns, numbers indicate the SPS concentration. Numbers on the upper left of the images indicate light dose (LD) in mJcm^{-2}.

The refractive index (RI) of solutions containing different concentrations of SPS or Ru was calculated in order to adjust the algorithm of the printer. While calculating the RI of gelMA solutions with different concentrations of SPS we found that the RI increases linearly depending on the amount of SPS present in the solution (R^2=0.9) while RI and concentration of Ru do not show a correlation (R^2=0.2) (Figure 5).

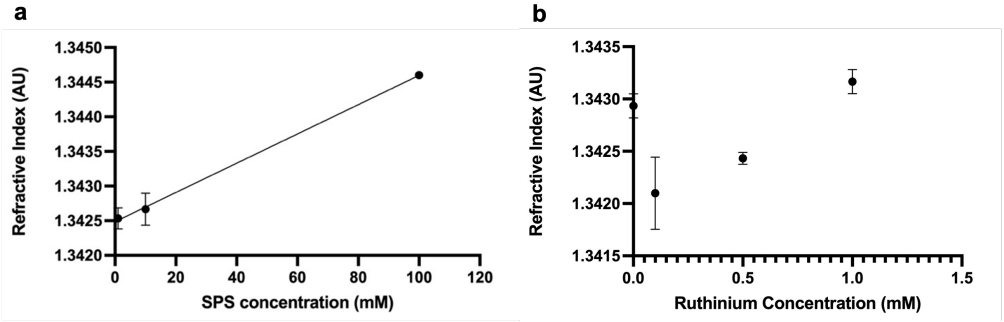

Figure 5: Sodium persulfate concentration affects the refractive index of hydrogels. (a) Refractive index of varying SPS concentrations. (b) Refractive index of varying Ru concentration. Refractive index was measured using an Abbe refractometer.

Once the concentration of Ru and SPS as well as the appropriate light dose were established, cells were added in the bioink to be printed. Two different cell densities were tested to establish the difference in resolution. The results are displayed in figure 6. The figure shows the small (1mm hole) and large features (2mm hole) of the disk. Both cell densities showed similar resolution, considering the formation of both small and large features. The lower cell density shows lower resolution in the formation of the small feature.

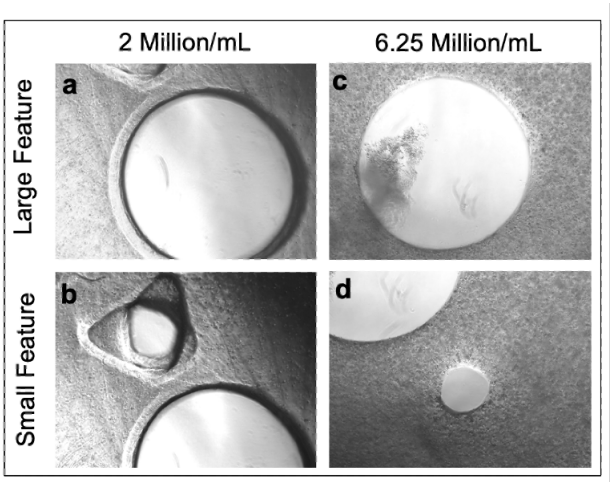

Figure 6: Cellular density minimally affects printing resolution of gelMA hydrogels crosslinked with RuSPS. (a) Microscope image of the large feature of the printed hydrogel encapsulated with 2 million hMSCs per mL (b) Microscope image of the small feature of the print of the printed hydrogel encapsulated with 2 million hMSCs per mL. (c) Microscope image of the large feature of the printed hydrogel encapsulated with 6.25 million hMSCs per mL. (d) Microscope image of the large feature of the printed hydrogel encapsulated with 6.25 million hMSCs per mL.

Further optimization of the prints encapsulating 6.25M cells/ml was conducted by altering the light dose. The results of this optimization process are displayed in figure 7. At 475mJ cm^{-2} only one one hole is created. The printed constructs were monitored over a period of 5 days. Measurements of the features within the prints revealed that features were significantly reduced in size compared to prints without cells embedded in the bioink (see appendix 6.1). Moreover, differences are also highlighted between the prints created at different light doses.

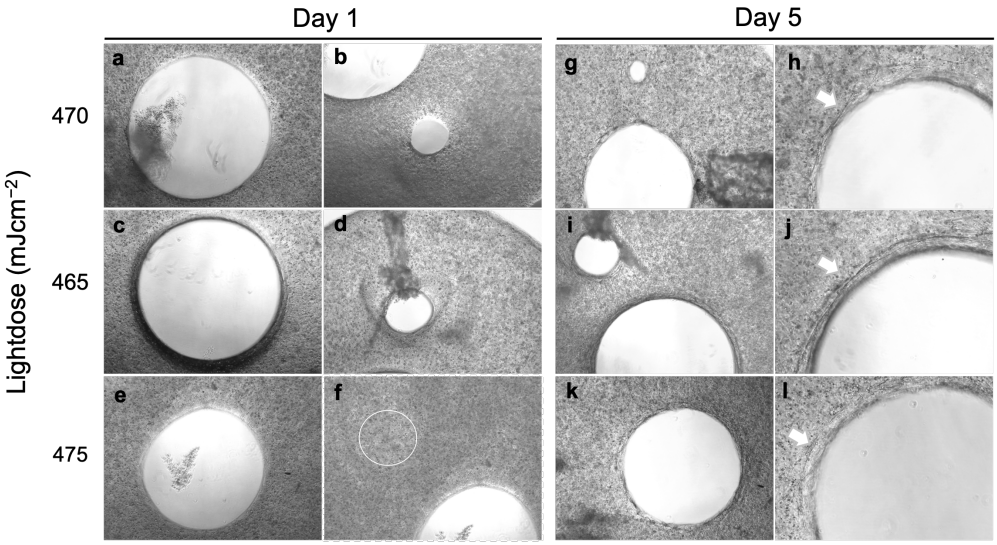

Figure 7: Shape fidelity can be maintained by adjusting the light dose in high cellular density printed constructs. (a-f) Cell-laden volumetric bioprinted gelMA hydrogel constructs at day 1. a,b Cell-laden constructs volumetric bioprinted at 470 mJcm^{-2}. c,d Cell-laden constructs volumetric bioprinted at 465 mJcm^{-2}. e,f Cell-laden constructs volumetric bioprinted at 475 mJ/cm^{-2}. (f) The dotted circle indicates the location of where the small feature should have been formed. (g-l) Cell-laden volumetric bioprinted gelMA hydrogel constructs at day 5 of culture. g,h) Cell-laden constructs volumetric bioprinted at 470 mJcm^{-2}. i,j) Cell-laden constructs volumetric bioprinted at 465 mJcm^{-2}. k,l) Cell-laden constructs volumetric bioprinted at 475 mJcm^{-2}. White arrows indicate location of cell spreading. Constructs were laden with hMSCs at 6.25 million cells per mL. Cell-laden constructs were kept in culture for 5 days. gelMA hydrogels were crosslinked with the RuSPS photoinitiating system.

3.1.3 Volumetric Bioprinting with varying GelMA content

Mechanical Properties The mechanical properties of the printed construct were compared to that of casted hydrogels with the same concentration of gelMA and photocrosslinking agents, gelMA 5%, Ru 0.1mM, SPS 10mM (Figure 8. The printed Gel-MA hydrogels observe a compressive modulus of 7.5 ± 0.41 kPA, 6.0 ± 0.53 kPa, 2.3 ± 0.24 kPa for 5%, 4% and 3% (w/v%) gelMA content respectively. The casted gels display compressive modulus of 5.5 ± 0.47 kPa, 1.6 ± 0.12 kPa, 1.5 ± 0,09 kPa for 5%, 4% and 3% respectively. Significant differences are observed between prints of different gelMA content and between casted gels of different gelMA contents. Significant differences are also present between prints and casts of the same gelMA content. The prints show a linear tendency, with lower gelMA content corresponding to lower compressive modulus. The trend is present in the casted gels however 4% casted gels show compressive modulus close to that of the 3% gels.

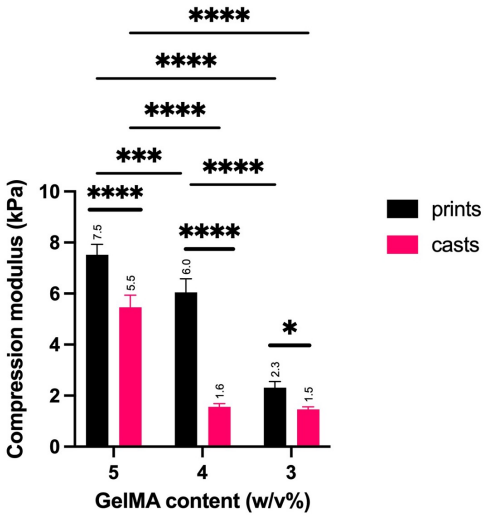

Figure 8: Compressive modulus of printed and casted gelMA constructs of different gelMA concentrations. Mechanical test on the printed and casted gels was performed using a dynamical mechanical analysis. ****Indicates significant difference between columns at the each end of lines ($p<0.0001$), *** indicates significant difference of $p<0.001$ and *indicates a significant difference of $p<0.05$

Biological Assays After evaluating the mechanical properties of the prints from different gelMA content we examined the effect this difference of stiffness would make to cell functionality. The constructs were monitored over seven days (figure9). The metabolic activity of these constructs was assessed by performing an alamar blue assay at day 1, 3 and 7. Significant differences can be observed between the two conditions at day 3 with the 3% gels showing significantly higher activity compared to the 5% gels. This trend continues at day 7, where 3% gels show higher activity compared to 5%.

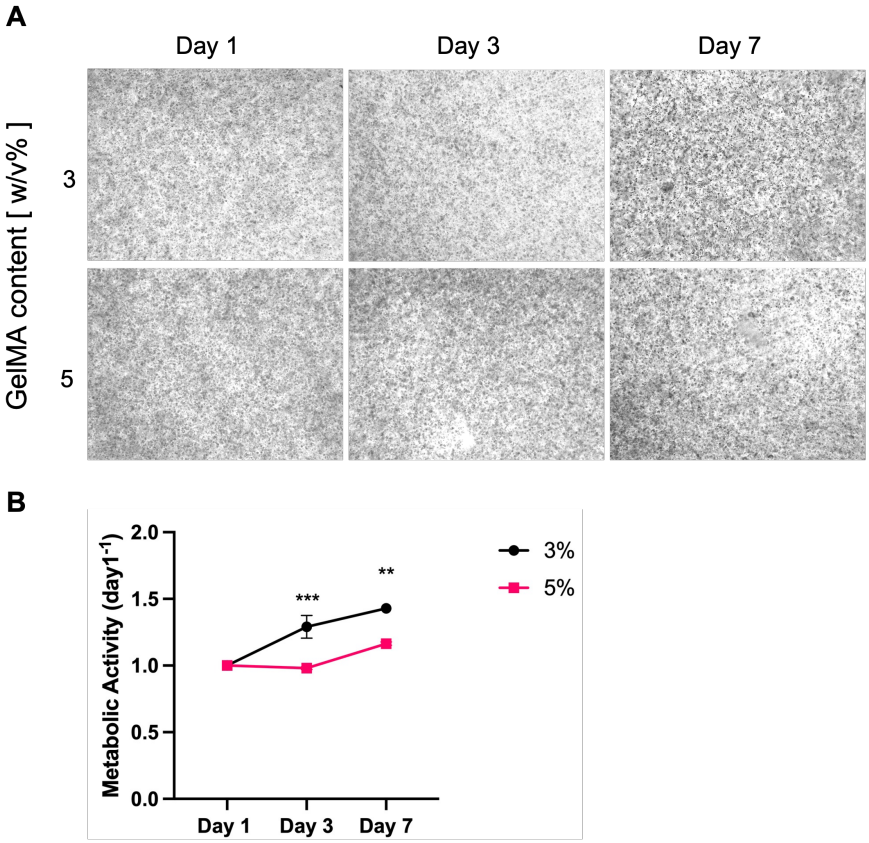

Figure 9: Lower gelMA concentration may promote cellular elongation and improve metabolic activity. A Microscope images of volumetric bioprinted cell-laden gelMA hydrogel constructs of different gelMA concentrations. B Metabolic activity of hMSCs encapsulated in volumetric bioprinted gelMA hydrogels of different gelMA contents. The cell-laden constructs were monitored over seven days. Metabolic activity was measured using an alamar blue assay. Metabolic activity was normalized to day 1 for each condition. The 3% group (black) refers to the gels fabricated with 3% gelMA concentration. The 5% group (pink) refers to the gels fabricated with 5% gelMA concentration. *** indicates significant difference compared to day 1 ($p<0.001$), ** indicates a significant difference compared to day 1 ($p<0.01$).

Viability in the different gelMA content gels was tested by performing a live/dead staining assay (Figure 10). At day 1, no notable difference in viability is observed between the different gelMA contents as both exhibit 80% viability (Figure 10 B). However at day 7, a significantly higher cell viability in the 3% gels (83%) is observed compared to 5% gels (26%) (Figure 10 B).

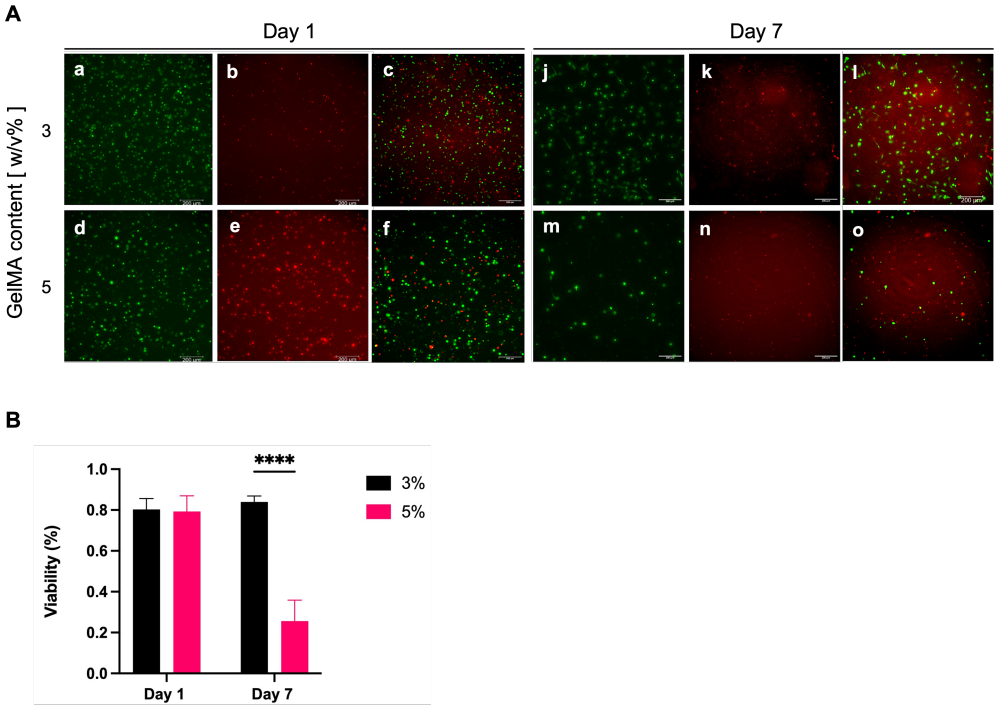

Figure 10: Tuning of material stiffness to improve cell viability in printed constructs. A. Live/Dead images of hMSCs encapsulated in 3 and 5% volumetric bioprinted gelMA hydrogels. Live cells are stained green, dead cells are stained red. (c,f) Merged images of live and dead images of the cell-laden construct at day 1. (l,o) Merged images of live and dead images of the cell-laden construct at day 7. B. Quantification of cell viability calculated based on the live/dead microscope images. The constructs were monitored over 7 days. ****Indicates significant difference between columns at the each end of lines ($p<0.0001$).

Metabolically, a significantly higher activity is observed at day 3 for 3% gels (figure 11). The 5% gels observe a dip in activity at day 3 but seem to recover between day 3 and day 7.

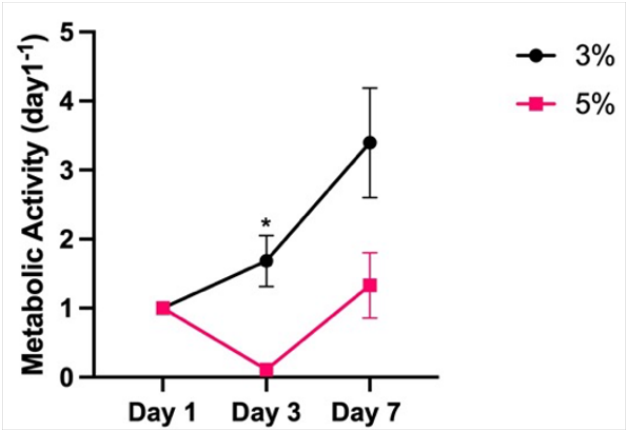

Figure 11: Tuning of material stiffness to improve cell functionality in printed constructs. Metabolic activity of hMSCs encapsulated in 3 and 5% volumetric bioprinted gelMA hydrogels..The constructs were monitored over 7 days. Metabolic activity was measured with alamar blue assay. Metabolic activity was normalized to day 1 for each condition. *indicates a significant difference compared to day 1 ($p<0.05$).

3.2 Anchoring Strategy

After finding the optimal method to anchor gels (see 2.10, hMSCs and ECFCs (stained dsRed) were encapsulated in 5% gelMA at a cellular density of 6.25M cells/ml (Figure 12). The anchors were monitored over 14 days. 5% gelMA hydrogels without anchors were used as control. Some connections seem to have formed in the 5% gels at day 7 which are maintained until day 14. Controls do not show connection or stretching.

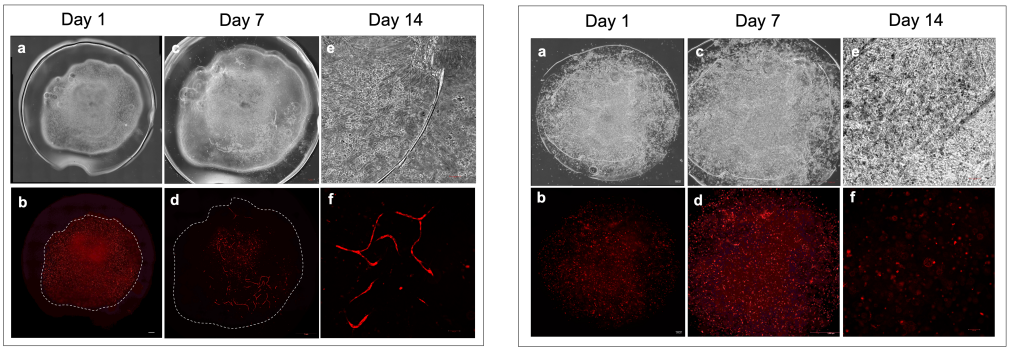

Figure 12: Anchoring cell-laden gelMA hydrogels may prevent hydrogel contraction. A hMSCs and ECFCs encapsulated in gelMA hydrogels then anchored in 15% gelMA. A. (a,c,e) Brightfield microscope images. (b,d,f) Fluorescent microscope images. B. Cell-laden gelMA constructs not anchored, used as controls. (a,c,e) Brightfield microscope images. (b,d,f) Fluorescent microscope images. ECFCs are ds Red stained. All constructs were monitored over 14 days. Images were obtained using a Thunder microscope. Dotted lines represent the border between cell-laden constructs and the 15% gelMA anchor.

The same anchoring process was applied to cells encapsulated in Cultrex BME (Figure 13), adapting the method to fit the gelation properties of this type of membrane (see 2.10). Few connections are formed at day 7 in both control and anchored gels. Day 14 shows better connections in control compared to anchored gel. Anchored gels seem to be only attached to the side of the 15% gelMA and have ruptured the gel leaving the middle of the anchor empty.

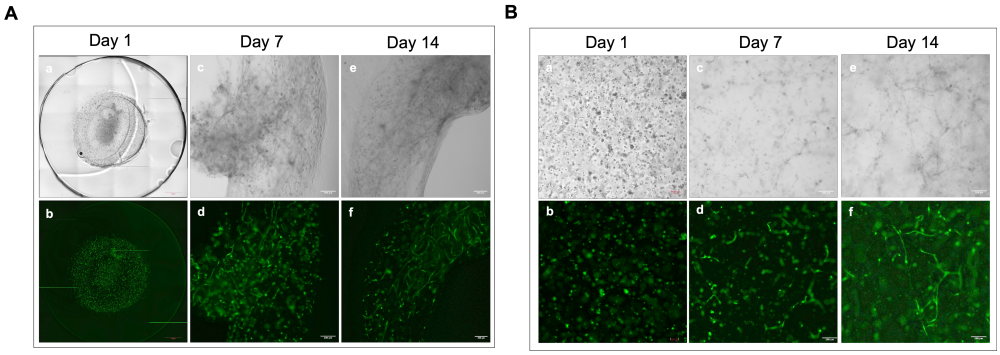

Figure 13: Anchoring cell-laden Cultrex BME constructs does not prevent hydrogel contraction. A. hMSCs and ECFCs encapsulated in Cultrex BME constructs then anchored in 15% gelMA. (a,c,e) Brightfield microscope images. (b,d,f)Fluorescent microscope images. B. Cell-laden Cultrex BME constructs constructs not anchored, used as controls. (a,c,e) Brightfield microscope images. (b,d,f) Fluorescent microscope images. ECFCs are GFP labeled. All constructs were monitored over 14 days. Images were obtained using a Thunder microscope.

3.3 Investigating other materials

First, the optimal concentration of gel content (w/v%) and crosslinking percentage was explored and tested through mechanical testing. Figure 14 A displays the compressive modulus of 5,4 and 3% gels with varying DTT concentration, mainly 4, 2 and 1mM. Lower concentrations of DTT show lower compressive modulus. Similarly, lower gel content shows lower compressive modulus. Within low DTT concentrations, 2 and 1mM, the compressive modulus is low regardless of the gel content. Sol-gel analysis of hydrogels with different gelNor content and DTT concentration was performed in order to evaluate the physico-chemical and mechanical properties of the constructs. Figure 14 B shows the mass swelling of the gels which shows a linear trend for the condition where 4mM DTT concentration was used, where an increasing mass swelling can be observed as gel content decreases.

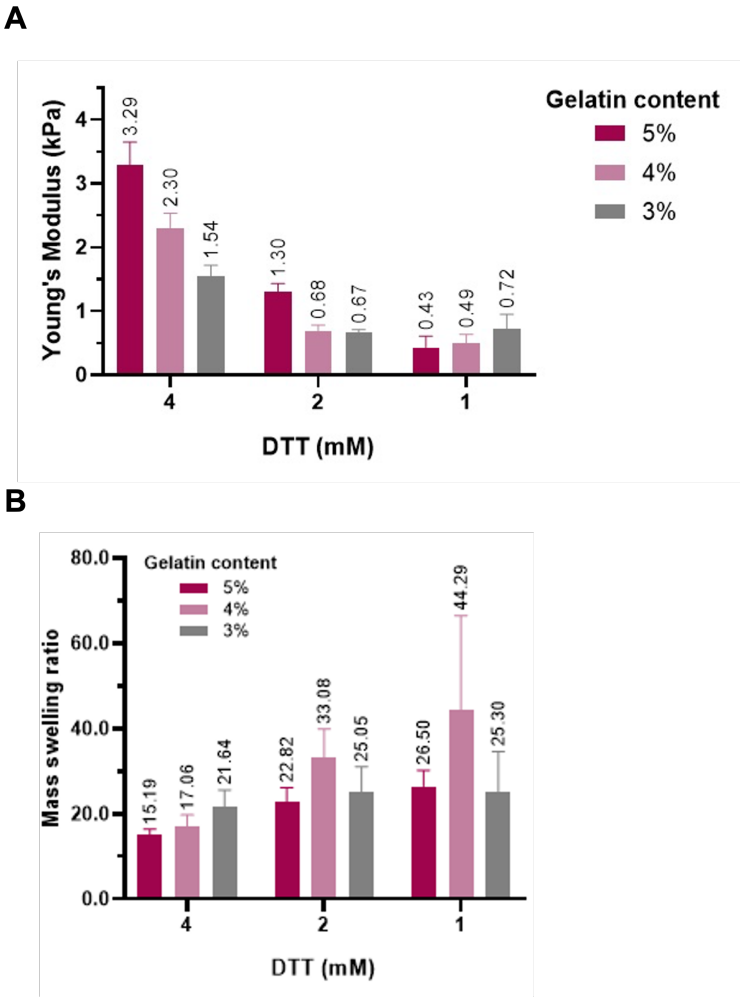

Figure 14: Physico-chemical properties of gelNor hydrogels fabricated using different concentrations of DTT and gelNor content. A. Compressive modulus of casted gelNor hydrogels using different gelNor content and DTT concentration. Compressive modulus was measured using a dynamical mechanical analysis. B. Mass swelling ratio q of gelNor hydrogels fabricated using different concentrations of DTT and gelNor content.

After exploring mechanical and physical properties of the hydrogels, we encapsulated hMSCs and ECFCs in 5% hydrogels, 100% crosslinked (7mM DTT) to examine the biological properties of this material (Figure 15. The cells did not show any improvements over the first 3 days post

encapsulation.

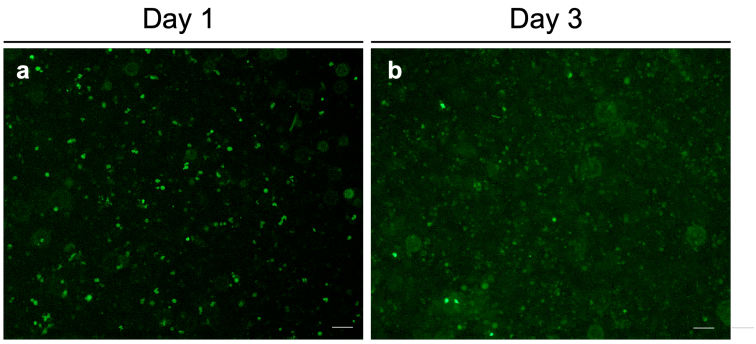

Figure 15: No proliferation of cells encapsulated in gelNor constructs. hMSCs and ECFCs encapsulated in 5% GelNor hydrogels. ECFCs are GFP labeled. The constructs were monitored for 3 days. GelNor Hydrogels were crosslinked DTT and LAP under UV light.

3.4 Investigating conditions for the bone marrow vascular niche

Since the goal of this study was to recreate an environment that most closely resembles the bone marrow niche, while promoting HSC maintenance and proliferation, we investigated several culture conditions for hMSCs and ECFCs based on conditions that HSCs thrive in. hMSCs and ECFCs were encapsulated in Cultrex® BME which is the standard for 3D culture of these cells. We investigated the presence or absence of serum in the EGM2 medium, the presence or absence of MMC, and the presence or absence of oxygen at different time points. Results are displayed in Figure 16. Significant difference in metabolic activity is observed at day 9 between the control and FBS with MMC condition (16 B). The control culture condition showed highest activity followed by the MMC with serum. The MMC with serum while showing high metabolic activity does not show high vessel formation. This is further supported by the results of the angiotool analysis. ECFCs formed long, interconnected networks suggestive of functional microvasculature. ECs in MMC conditions, however, displayed reduced network formation with limited cell-cell connectivity. MMC conditions also led to a marked decrease in average vessel length compared to control.

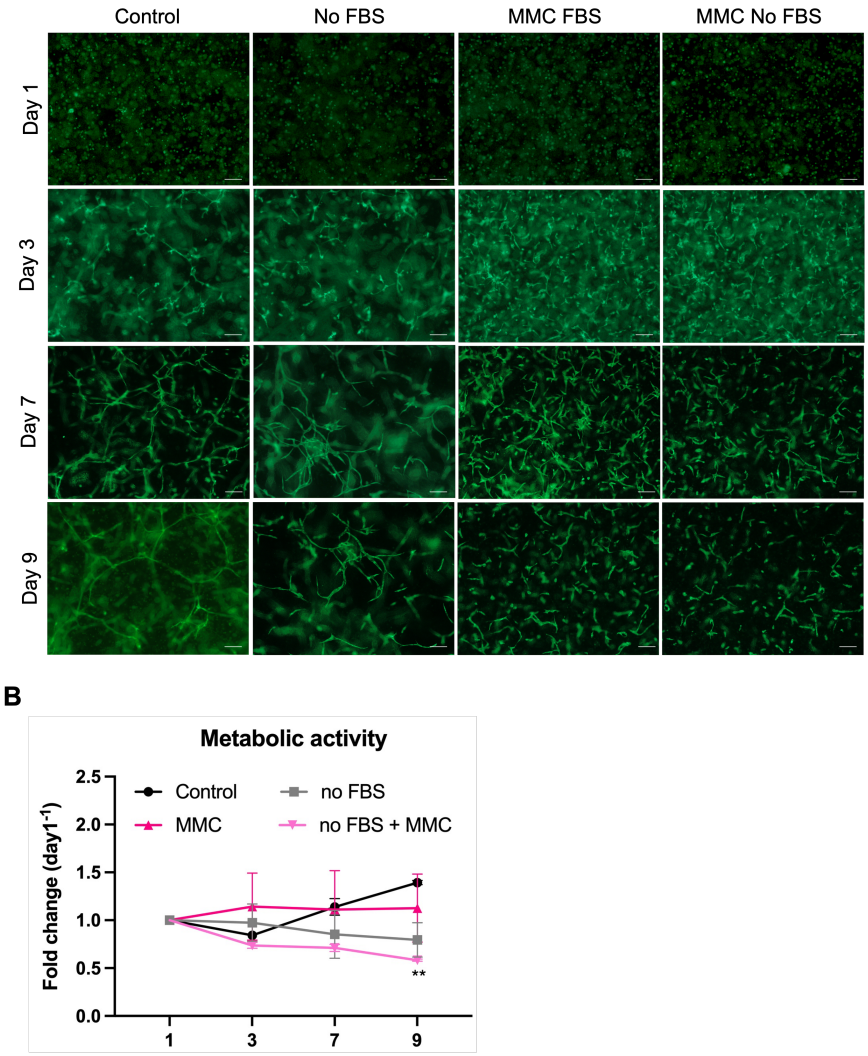

Figure 16: MMC may promote niche cell proliferation. A. Vasculogenesis of ECFCs and hMSC co-culture in Cultrex BME constructs. B. Metabolic activity of hMSC and ECFC co-culture in Cultrex. Metabolic activity was measured with alamar blue assay. Metabolic activity was normalized to day 1 for each condition. The constructs were monitored over 9 days. Control group consists of the cell-laden constructs cultured in EGM2 medium. No FBS group consists of cell-laden constructs cultured in EGM2 without addition of FBS. MMC FBS group consists of cell-laden constructs cultured in medium containing macromolecules and FBS. MMC no FBS group consists of cell-laden constructs cultured in medium containing macromolecules and FBS. ECFCs are GFP labeled. Scale bar = 200m. ** indicates a significant difference compared to day 1 ($p<0.01$).

The bone marrow niche environment is characterized by its hypoxic gradient. A hypoxic gradient is present within the bone marrow niche suggesting HSC may perform better in low oxygen conditions. We investigated the effect of hypoxia on hMSCs and ECFCs co-culture. This condition was introduced from day 1 onwards or from day 3 onwards (Figure 17). Significant difference in metabolic activity is observed at day 9 between control and hypoxia at day 3 (Figure 17 B). Environments where hypoxia was introduced from day 3 onwards show significantly higher metabolic activity compared to a normoxic environment and to a hypoxic environment introduced at day 1. Cells seem to be forming connections in all three conditions, as can be observed in figure 17.

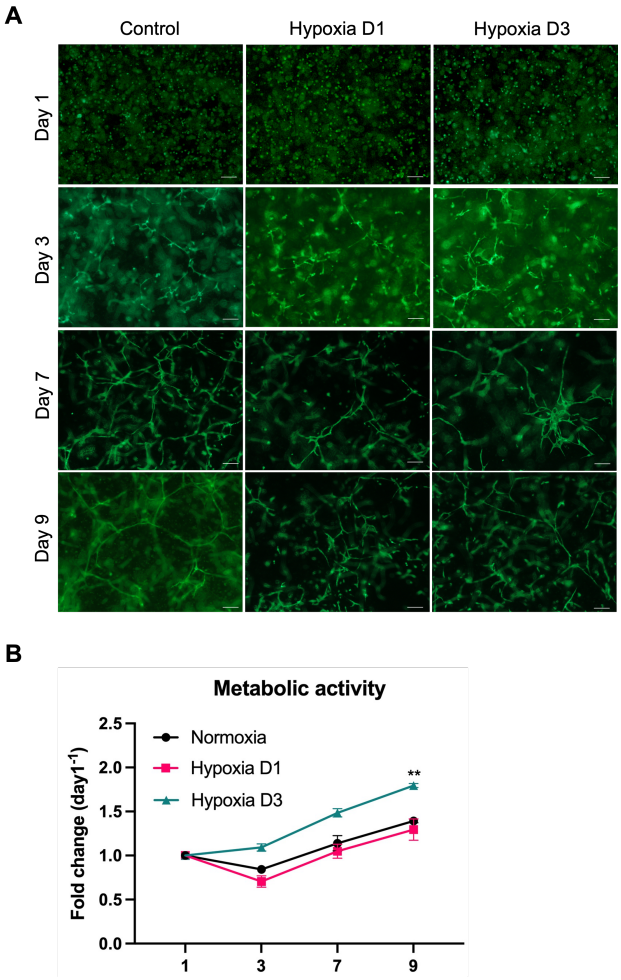

Figure 17: Niche cells are functional in hypoxic environments. A. Vasculogenesis of ECFCs and hMSC co-culture in Cultrex BME constructs. B. Metabolic activity of hMSC and ECFC co-culture in Cultrex in hypoxic conditions. Metabolic activity was measured with alamar blue assay. Metabolic activity was normalized to day 1 for each condition. Normoxia refers to the constructs that were kept at normal oxygen levels. Hypoxia D1 refers to the constructs that were placed in hypoxia from day 1 of the culture onwards. Hypoxia D3 refers to the constructs that were placed in a hypoxic environment from day 3 onwards. ** indicates a significant difference compared to day 1 ($p<0.01$).

To establish conditions for the co-culture of vascularized structures and HSCs we investigated the effect of different medium blends of EGM2 and StemSpan and the delivery of these media at different time points. For this, we encapsulated hMSCs and ECFCs in Cultrex BME droplets in a well plate and proceeded to add the different media to the droplets. We delivered EGM2 alone, StemSpan alone or a 1:1 ratio of EGM2 to Stem Span from day 1 or from day 3 onwards, totalling 4 different conditions. We evaluated endothelial cell network formation over a period of 12 days. Results are displayed in figure 18

In the EGM2 condition, connections start forming faster from day 3 (Figure 18 A). At day 7, EGM2 and Stem Span show better endothelial cell connection compared to the combination of media which promotes less connectivity. Vessel formation in the constructs was then analyzed using a computational tool for quantitative analysis of vascular network parameters (AngioTool,

[32]). EGM2 observes an increase in total vessel length (Figure 18 C), but all other conditions show lower vessel length. There is a trend in increase of total vessel length in both EGM2 and StemSpan conditions. At day 12 as expected EGM2 gels have the denser EC networks. On the other hand, mixture does not lead to consistent vessel formation or maintenance. Concerning the junction density (Figure 18 B), more connections but the vessels are shorter at day 3. Between day 3 and day 12 there may be some kind of reorganization, which is observed by a decrease in junctions because vessels are forming. After the vessels are formed, there is an increase in junction density.

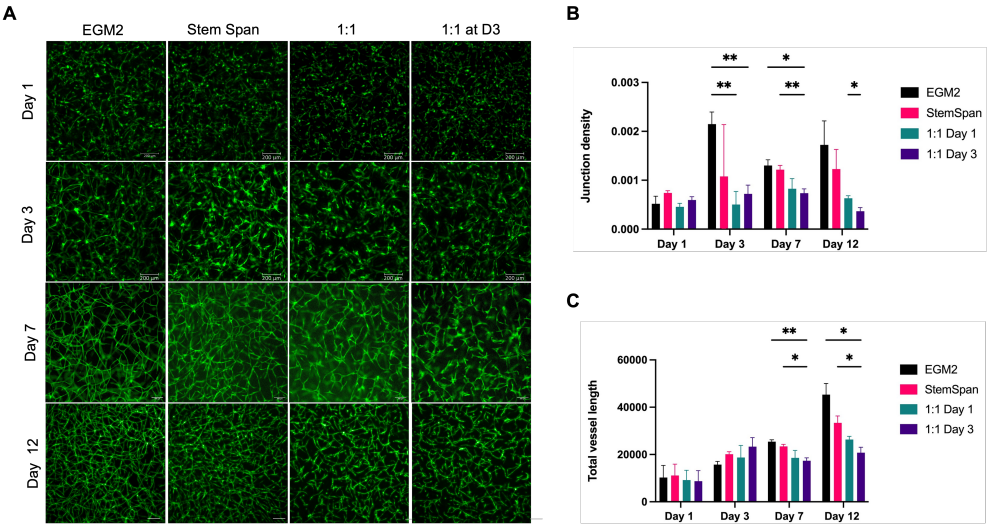

Figure 18: Endothelial cell network formation under different media formulae. A Microscope images of samples in the different medium conditions. ECFCs are GFP labeled. B Junctions density and C Total vessel length of microcapillaries observed. Constructs were monitored over 12 days. 1:1 D1 corresponds to condition where the combination medium (EGM2 and StemSpan 1:1 ratio mix) was used for the co-culture from day 1 onwards. 1:1 D3 corresponds to the condition where the combination medium (EGM2 and StemSpan 1:1 ratio mix) was used for the co-culture only from day 3 onwards. ** indicates significant difference between conditions at the end of the line ($p<0.01$); * indicates significant difference between conditions at the end of the line ($p<0.05$). Scale bar = 200m.

The medium blends observe similar levels of metabolic activity while EGM2 and Stemspan have very different metabolic profiles (Figure19). EGM2 significantly improved the activity of cultures after day 3. Stemsapn decreased considerably the activity of cultures and remained stable throughout the culture time. Medium blends did not show to impact the activity of the cultures over time. Taking EGM2 as the gold standard, all the other conditions decreased the metabolic activity in the culture with stemspan showing the worst activity. However, it seems the blend of the two media, mitigates the negative effect of stemspan on cellular metabolism.

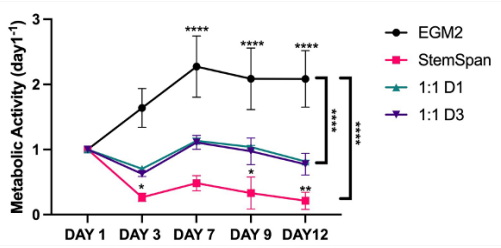

Figure 19: Impact of different media formulae on metabolic activity of hMSCs and ECFCs co-culture. Constructs were monitored over 12 days. 1:1 D1 corresponds to condition where the combination medium (EGM2 and StemSpan 1:1 ratio mix) was used for the co-culture from day 1 onwards. 1:1 D3 corresponds to the condition where the combination medium (EGM2 and StemSpan 1:1 ratio mix) was used for the co-culture only from day 3 onwards. **** indicates significant difference compared to day 1 ($p<0.0001$); ** indicates a significant difference compared to day 1 ($p<0.01$); * indicates a significant difference compared to day 1 ($p<0.05$). **** on vertical lines indicate significant difference between conditions at the end of the line.

4 Discussion

Biofabrication technologies have made major advances in regenerative medicine as effective tools for tissue regeneration [20, 21, 5, 22, 23]. More specifically, cutting edge technologies such as VBP have truly transformed the field as VBP allows for the rapid development of whole cell-laden complexes of any size and architecture in tens of seconds [33]. Such sophisticated advancements become particularly relevant when trying to emulate a complex environment that is the bone marrow. This microenvironment not only contains cellular key players in the maintenance of HSCs, its mechanical properties serve as cues to the functioning of these stem cells responsible for the rise of all blood cell type lineages. Recreating this environment *in vitro* is crucial to establish diseases of the bone marrow but also to deepen our understanding of this tightly regulated microenvironment. This project aimed at the biofabrication of a vascularized bone marrow model for bone marrow engineering which was achieved by bioprinting a hydrogel with bone marrow mimicking properties, and establishing conditions for the co-culture of vascularised structures and HSCs.

4.1 Development of Bioink for Volumetric Bioprinting of Bone Marrow Model

In this study, we developed a gelMA based hydrogel crosslinked with a visible light photoinitiating system for VBP. Characterization and evaluation of hydrogels with different gelMA concentrations revealed that lower polymer concentration more closely replicates select properties of the bone marrow. Moreover, gelMA concentration is revealed to be critical for cell spreading and stretching in gelMA embedded MSCs.

4.1.1 Photoinitiating systems: Volumetric Bioprinting using a visible light initiating system

Successfully printing with LAP as photoinitiator showed it was possible to print at high cell density, resembling the cell density present in the bone marrow bringing the model one step closer to mimicking this complex environment. The printed constructs were stable for 7 days while showing support for adhesion, spreading and proliferation of hMSCs within the construct. It also demonstrates that the light dose previously reported by [21] could be applied for a different cell line and cell density.

Few photoresponsive hydrogels and photoinitiating systems have been reported to successfully print with the volumetric bioprinter. The most commonly used is LAP due to the radicals it generates under UV light (the wavelength used in the printer is 405 nm). After being exposed to the laser beam in the printer, the constructs have to undergo additional crosslinking in 0.1%w/v LAP in PBS solution in a UV crosslinker, increasing the exposure to UV radiation. However, it has been demonstrated that UV radiation may cause cellular DNA and tissue damage in the long term [34]. Ru can be coupled to SPS to create a visible light initiating system. When irradiated with visible light, the photo-excited Ru donates electrons to SPS which provokes its dissociation into sulfate anions and sulfate radicals. The subsequently generated radicals can crosslink gelMA by propagating through the methacryloyl groups [22]. RuSPS not only crosslinks the methacrylates in gelMA it is also able to crosslink tyrosines which is valuable for decorating the gels with biological molecules that also contain tyrosines, making this material further customizable. Moreover, this system has been shown to have a better penetration depth and cytocompatibility when compared to commonly used UV-based initiator systems [5]. Using the RuSPS photoinitiating system to print constructs with the volumetric bioprinter was never previously reported since it has a high molar absorptivity at 450nm compared to other photoinitiating systems, such as LAP, while the peak excitation source of the printer is at 405nm.

We showed that printing small features with RuSPS is possible. The optimization process revealed that while keeping the Ru concentration constant, the printed constructs were less stable with increasing amounts of SPS. The adequate light dose is nearly twice as high as the light dose used for constructs printed with LAP. Since the RuSPS system is poorly excited by the 405nm laser of the printer, a higher light dose is necessary to crosslink the bioink. The concentration of SPS is 100 times that of Ru. Previous work using this photo initiating system showed that 0.1/1 RuSPS (Mm/Mm), with a minimum of 5 min exposure time was required to fabricate stable casted hydrogels [5]. Higher concentration of SPS might be needed to generate enough radicals to crosslink the gelMA when irradiated by the laser of the printer which has an excitation peak at 405 nm.

Moreover, by printing 6.25 million cells/mL, we demonstrate an appropriate cell density for promoting vessel formation. However, shape fidelity is reduced in prints with cells compared to printed constructs without cells. Printing with 2 million cells /mL and 6.25 million cells/mL demonstrated that similar resolutions can be achieved regardless of the cellular density within the construct. Adjusting the light dose could be sufficient to account for the small differences in resolution. The printed cell-laden hydrogels showed to support cell spreading and contraction within the printed construct, exhibiting interaction between the cells and the material. This suggests that using gelMA and RuSPS photocrosslinking system for VBP gives the cells the ability to reorganize their network and regulate the matrix, showing activity and viability within the construct. This gives an indication of the behavior of the cells while interacting with the structure of the prints. These cell-laden printed constructs provide useful insight regarding potential areas for vessel formation when examining where the cells spread the most. Cells show stretching and interaction around holes within the disk as well as on the outer band of the print. These results demonstrate the potential effect the shape of the print has on cell function. This highlights yet another advantage of the volumetric bioprinter which allows for the generation of complex and free form structures. This cutting edge technology could make it possible to promote different cell phenotypes by printing specific structures inspired by the natural structures present during fetal development or adulthood depending on the phenotype desired.

4.1.2 Mechanical Tuning of gelMA hydrogels with Visible Light Initiating System

Developing a bioink with printing capabilities that also provides the specific conditions needed to emulate the bone marrow environment and promote cell self-assembly remains challenging [23]. Different factors have to be taken into consideration such as the stiffness of the bone marrow perivascular microenvironment which ranges between 0.1 and 3kPa[13]. Small changes in material stiffness and polymer concentration have been shown to significantly affect the quality of the resulting microcapillary network [23]. Softer but maniable gels are required to achieve this goal and promote vessel formation. In an attempt to tune the mechanical properties of the gelMA hydrogels, we tested different gelMA content mainly 5, 4, and 3% (w/v%). VBP with lower gelMA content than 5% had not been reported before.

Mechanical testing revealed that 3% gelMA hydrogels most closely resemble the stiffness of the bone marrow environment compared to higher gelMA content. We compared the stiffness of casted gels versus printed gels which showed that the printed gels are stiffer than the casted gels, making the lower gelMA content desirable for printing. Thus, through adjusting the macromer concentration we were able to fine tune the mechanical properties of gelMA hydrogels to mimic bone marrow stiffness while still conserving a material that can be handled. The difference in compressive modulus between the prints and the casts for each gelMa content may be explained by the fact that when printing these construct, the light dose for each gelMA content is adjusted, higher light dose for lower gelMA content (see appendix 6.3) whilst all the casted gels regardless of gelMA content undergo visible light crosslinking for 5 minutes. Adjusting for this difference could be investigated by lowering the curing time based on the gelMA content.

We found that viability and metabolic activity are improved in 3% gels. Moreover, higher cell elongation is visible in 3% gels which is particularly important for vessel formation. The mechanical properties of gelMA hydrogels are related to the macromer concentration according to the power law [35]. The gradient changes in the bone marrow stiffness are caused by its inhomogeneity. In contrast to the perivascular niches surrounded by VEC and adipocytes, which are significantly softer in stiffness, the endosteal region close to the bone surface is densely populated by bone-cell progenitors and enriched with high levels of fibronectin [13]. Recreating appropriate stiffness to mimic the bone marrow perivascular niche is crucial as these biophysical cues can affect the behavior of cells such as differentiation, migration and adhesion of cells and alter the fate of stem cells [13].

Of important note, a different batch of gelMA was used to perform the second assay (Batch 11) which dramatically changed the light dose required. Indeed, a significantly lower light dose was needed to crosslink the gels which led to over polymerized and thus stiffer printed constructs which in turn affects cellular behavior. This difference illustrates the considerable batch to batch variability but more importantly the unpredictability of natural materials.

4.1.3 Sodium Persulfate Concentration Affects Refractive Index of hydrogel Solution

The RI of a solution provides information regarding potential tunings to obtain the optimal light dose and thus reach optimal crosslinking. If the SPS concentration is decreased, the kinetics of the reaction is lowered. On the other hand, if the SPS concentration is increased, in turn the kinetics of the reaction is also increased along with the RI which can then be corrected by the algorithm of the printer. Although the Ru does not affect the RI, it does however interfere with the absorptivity

which can also be adjusted by the algorithm of the printer. This information becomes relevant since rapid polymerization kinetics of photocrosslinkable materials is key to achieve accurate prints in VBP [21]. Cells and other sub-cellular structures can change the course of incident light and may lower the printing resolution [21]. The projected images will be distorted by scattered light, increasing the light dose in areas of the volume adjacent but outside of the area to be printed[21]. Understanding the parameters that contribute to changes in RI is relevant to produce accurate prints and lower the risk of off-target polymerization. We showed that SPS has an impact on the RI and should be taken into account when using RuSPS with the VBP as this measure can be adjusted through the algorithm of the printer.

Taken together, the results obtained from using the gelMA and RuSPS formulation for VBP suggest that lower gelMA content could promote niche cell proliferation and function, highlighting the importance of tuning the biomaterial mechanical properties to mimic stiffness in the native tissue.

4.2 Anchoring VBP Printed Cell-laden Constructs Could Avoid Gel Contraction

MSCs and ECFCs tend to contract the hydrogel constructs they are encapsulated in. This phenomenon usually forces the hydrogels constructs to detach which in turn results in loss of cell functionality. An anchoring method was designed in an attempt to prevent this phenomenon. Although connection and vessel-like structures can be observed in the anchored gels, the control gels do not show any sign of cell stretching or assembly. The lack of functionality observed in the control gels may be explained by the cell type used. ECFCs stained with dsRed had a significantly lower cell viability and function in culture and other experiments conducted.

A similar anchoring method was applied to cells encapsulated in Cultrex BME, since proving this method avoids gel contraction in the standard of use for 3D culture of endothelial cells and vascularized constructs, would be beneficial to any 3D culture set up rather than only volumetric bioprinted constructs. Although, contraction of the gel still occurred, better proliferation could be obsvered in comparison to the gelMA encapsulated anchored hydrogels. This could be explained by the difference in cell type used (ECFCs dsRed for gelMA constructs and ECFCs GFP labeled for Cultrex BME constructs) or most probably the type of material used to embed the cells (gelMA versus cultrex) since Cultrex is the standard for 3D culture of endothelial cells and vascularized constructs.

Although further work is needed, the strategy elaborated in this study paves the way for anchoring casted gels or more generally 3D printed hydrogel constructs to avoid gel contraction.

4.3 Investigating other materials: Gelatine Norbornene

Scaffold-based strategies adopting hydrogels as biomaterials for tissue engineering offer a number of advantages due to their highly hydrated polymeric network and their structural similarity to native ECM [23]. Although gelMA has been widely used as photocrosslinkable material, it holds numerous drawbacks. The moieties in gelMA are non-degradable indicating that any link formed cannot be degraded which does not constitute a tailorable environment for cells to thrive in. Moreover, controlling the crosslinking percentage is challenging in gelMA hydrogels as this material can create double bonds and crosslink itself. Gelatine norbornene (GelNor) emerged as a promising material. The Norbornene in gelNor masks the cleavable metalloproteinase (MPP1) sites and therefore allows

the cells to degrade the collagen to their liking which ultimately promotes better vessel formation. Soliman and colleagues [23] used gelNor hydrogels to promote vascularization in biofabricated constructs. Furthermore, in gelnor based hydrogels the crosslinker agent, DTT is the limiting factor, the cross linkage percentage can thus easily be changed based on the concentration of DTT use since the norbornene molecules have a 1:1 crosslinking ratio. Moreover, norbornene can crosslink any compound that contains a thiol group. Most protein found in the body containing cysteine will also contain a thiol group [36].

4.3.1 GelNor Hydrogel Mechanical Properties Mimic Bone Marrow Stiffness

These hydrogels constructs aim to mimic the bone marrow environment which includes its stiffness. The bone marrow stiffness ranges between 0.1 and 3kPa. Mechanically tuning gelNor hydrogels was conducted by testing different concentrations of DTT and gelNor content. Nearly every gelNor hydrogel fabricated shows stiffness within the desired range except for the 5% gelNor crosslinked with 4mM DTT (3.29kPa). Lower stiffness is an advantage to better mimic the bone marrow environment, however these gels should still be easily manipulated. Moreover, 5 and 4% hydrogels have more binding sites, which is advantageous when decorating the gels with cells. In this study we showed that most of the gelNor hydrogels fabricated observe a wide range of stiffness and it is possible to modify and adjust their crosslinking density making this material an ideal candidate for supporting and promoting vascularization in the bone marrow model.

The inconsistencies observed in compressive moduli in the 1mM gels might be due to the gels being already too soft for the DMA to accurately measure the stiffness. These results might correspond to the DMA clamp measuring the metal and not the hydrogel stiffness. The initial static force applied is very low (0.001N), which corresponds to the limit of the measuring tool. When a gel is too soft, the measurements might not be as accurate.

The swelling ratio is the proportional increase in the weight of the hydrogel brought on by water absorption. As the network density in hydrogels decreases it leaves more space for water. Lower gel contents such as 3%, is thus expected to swell more compared to gels with higher gel contents which have denser networks. These measurements give information regarding the fragility of the gels. Inconsistencies in the 1 and 2mM DTT conditions might be due to the loss of gel while transferring them between eppendorfs and well.

While this material showed promising mechanical and physical properties, cells embedded in the gelNor hydrogels showed no signs of proliferation as viability was severely impacted even after one day of encapsulation. Numerous failed attempts at understanding the cause of poor cell survival led to abandoning the use of the material for cell encapsulation.

4.4 Investigating Conditions for the Bone Marrow Vascular Niche

This project aimed at fabricating a vascularized bone marrow model for which we needed to establish conditions for the co-culture of vascularised structures which ultimately would promote HSC biology. Niche cells play an important role in supporting HSCs within the niche. Vascular cells within the niche promote HSC proliferation and differentiation through secreted important cytokines such as stem cell factor (SCF) and express proteins essential for HSC function (Cx43 & E-selectin) [2]. Perivascular cells also support HSC maintenance and regeneration. ECs and hMSCs are cultured

in different conditions compared to HSCs. Thus, to establish conditions for the co-culture of vascularized structures and HSCs the effect of several conditions on the culture of hMSCs and ECFCs was investigated. These conditions were chosen based on their potential a role in HSC maintenance and/or help in emulating the bone marrow microenvironment through a 3D model.

4.4.1 Presence of Serum in Culture Medium is Essential for Vessel Formation

It is common practice not to add serum in the medium when culturing HSCs. On the other hand, MSCs and ECFCs are always cultured in a serum environment. While investigating the difference between serum and serum free environments for the co-culture of hMSCs and ECFCs, we found that cells functioned significantly worse without serum. The importance of serum to obtain functional cells forming vessels is thus highlighted by the results obtained.

4.4.2 Macromolecular Crowding Promotes Niche Cells Proliferation

A number of cytokines are commonly added to HSCs culture medium for enhanced proliferation. However, this leads to rapid expansion and exhaustion of HSC stemness potential. Adding macromolecules into the medium could help the cells attain the cytokines without exhausting their pool of stem cells. The macromolecules would occupy space in solution, making the cytokines available to the stem cells in a sustainable fashion. This method referred to as MMC is generally described as the "volume of a solution that is excluded to the center of mass of a probe particle by the presence of one or more background particles in the medium" according to the excluded volume effect [37]. MMC impacts the solution by converting biopolymers into their functional states, buffering the effect of crowded settings on biological function, and making macromolecular transition complexes stronger with longer half-lives (e.g., enzyme-substrate) and resulting in greater product [37]. The addition of the inert crowders may confine the active elements present in the microenvironment by taking up a sizable portion of the medium, leading to associations and reactions [37].

Absence or presence of serum was also tested on top of MMC or no MMC. In serum-free environments ECFCs are expected to have a lower proliferation rate. However, MMC could help the cells reach GFs made more available which could compensate for the lack of serum. In general, MMC could help transit from full serum to serum free media and protect the cells and improve functionality. The results obtained show the importance of serum to obtain functional cells forming vessels. Although not functional, hMSCs and ECFCs cultured in MMC with serum showed increased cell number, which could be explained by an increased cell response to growth factors made available.

4.4.3 Niche cells are functional in hypoxic environments

Low oxygen tension is characteristic of the HSC niche as it is necessary for HSC quiescence and self-renewal in the hematopoietic system. Most quiescent and primitive HSCs are found in hypoxic, poorly perfused areas of the bone marrow [38]. Such circumstances cause cells to express high quantities of hypoxia inducible factor 1alpha (HIF-alpha) and force a switch from mitochondrial oxidative phosphorylation to glycolysis [9]. The metabolic state of a cell is crucial in deciding whether it divides, differentiates, or stays quiescent. When adult stem cells mature and when cells are reprogrammed to a pluripotent state, there is a change in the balance between glycolysis, mitochondrial oxidative phosphorylation, and oxidative stress [9]. Endothelial cells obtain their energy mainly from glycolysis at a very high pace [39]. In hypoxia, these cells consume large amounts of glucose which suggests an increased demand in nutrients. It is thus necessary to provide

glucose in quantities large enough to support this fast pace consumption which can be achieved by frequent media change.

Our results show that introducing hypoxic environments at day 3 may be beneficial for culturing niche cells. These findings suggest that the cells may function better if introduced to a hypoxic environment at a later time point. Leaving the cells time to adapt to their environment first proves to be beneficial if introducing a hypoxic environment is necessary which could be the case when culturing MSCs and ECFCs with HSCs within the same environment.

4.4.4 Negative effect of StemSpan on Cellular Metabolism can be Mitigated by EGM2

To establish conditions for the co-culture of vascularized structures and HSCs we investigated the effect of different medium blends of EGM2 and StemSpan and the delivery of these media at different time points. For this we encapsulated hMSCs and ECFCs in Cultrex droplets. We delivered EGM2 alone, Stem Span alone or a 1:1 ratio of EGM2 to Stem Span from day 1 or from day 3. EGM2 and StemSpan have complex but different compositions. EGM2 contains growth factors that help vessel formation whereas Stemspan contains inflammatory cytokines and proteins which may have an impact on endothelial network formation. It is important to establish a medium for the co-culture of vascular cells and HSCs so understanding their behavior in response to a medium usually used for HSCs expansion may be a first step towards that goal.

The metabolic activity results obtained suggest that niche cells cannot be cultured in StemSpan medium. However, these cell types still showed considerable activity when this medium was used in combination with the preferred medium, EGM2. Surprisingly, no significant difference was observed between the conditions where the combination medium was introduced at different time points. In fact, both conditions follow a similar metabolic activity trend over the 12 days. Introducing the combination at different time points should have an effect on the co-culture. More specifically, the condition where the combination medium was only introduced at day 3 should show similar activity to the control EGM2 until day 3 since the cells were only exposed to StemSpan at day 3. From a vessel network perspective, Stem Span medium show functional vessel formation, with high junction density and vessel length compared to combination medium conditions. Stem Span medium contains inflammatory cytokines which could trigger a metabolic switch in the ECFCs. Indeed, in ECs metabolism, glycolysis is the predominant glucose utilization pathway and contributes to the majority of total ATP produced. This preference for glycolysis proves to be advantageous as it maximizes the delivery of oxygen to perivascular cells and tissues while minimizing production of reactive oxygen species (ROS) through mitochondrial oxidative phosphorylation [40].

The endothelium is the first line of defense in the vasculature. Inflammatory stimulation has been shown to activate quiescent ECs to produce pro-inflammatory molecules and ROS. While this protects the vasculature from infection it also leads to major disruption in vascular integrity through increased inflammation and a metabolic switch in EC [41]. Oxidative phosphorylation and the pentose phosphate pathway are activated as homeostatic anti-inflammatory mechanisms. These inflammation-related metabolic changes also known as immunometabolic phenotypes might come into play when ECFCs are exposed to inflammatory cytokines in Stem Span medium.

An additional explanation for differences observed in metabolic activity compared to vessel formation may be that the metabolic activity reflects that of the hMSCs in culture which do not thrive metabolically in Stem Span. This would explain the difference observed between the vessel-like

structures formed and the metabolic activity. The ratio of ECFCs to hMSCs is 1 to 6, making the hMSCs population much more substantial compared to the ECFCs. Thus, even though vessel-like networks are forming, the metabolic activity may represent that of the hMSCs which outnumber the ECFCs. Staining of the hMSCs may help understand the behavior of these cells in the environment.

4.5 Conclusion and Future Perspective

The aim of this project was to investigate conditions for the fabrication of a bone marrow vascularized model. We developed a gelMA hydrogel combined with a visible light crosslinking system using RuSPS for VBP of cell-laden constructs with high shape fidelity in the presence of high cell density. We showed the possibility for fine tuning of the mechanical properties of gelMA hydrogels to match that of the bone marrow and promote cell functionality and viability. Lowering the gelMA concentration mimicked the mechanical properties of bone marrow tissue, and supported cell viability during cell culture of key primary bone marrow microenvironmental cells, found in the perivascular region. Thus, this bioink offers a foundation for modification with bioactive factors and tissue-specific components to enhance further bone marrow mimicry. Moreover, a stiffness gradient between endosteal and perivascular niches reigns within the bone marrow, and contributes to cellular behavior such as differentiation and adhesion of cells. Further research should consider embedding niche cells through the stiffness gradients emulated by the different gelMA layers, and examining the cellular behavior in response to the differences in matrix stiffness to understand the complex cellular interactions within the bone marrow niches but also the interactions between niche cells and their environment.

To recreate as closely as possible the bone marrow environment, we explored a novel material, gelNor. This material showed promising mechanical properties as we showed it is possible to fine tune the stiffness of the gels by adjusting gel content, and crosslinking density by manipulating the DTT concentration. However, when encapsulating cells in this material to show cellular behavior with optimal concentration of gel and crosslinking density, we observed that certain components within the gels appear to be toxic to the cells. Further investigation is required within the gelnor synthesis process to understand which part of the process might be toxic for the cells.

Additionally, we investigated strategies to mimic the natural conditions of the bone marrow perivascular niche environment. More specifically, conditions for the co-culture of hMSCs and ECFCs were elaborated. First, the necessity for serum in the medium environment for functional vessel formation was highlighted. However, when MMC was added to the culture medium, results revealed that MMC could help transition from serum to serum-free environment by promoting access to GFs and ultimately enhance cell proliferation. Finally, results from this study revealed that although EGM2 remains the most relevant for the co-culture of MSCs and ECFCs compared to StemSpan medium, this research showed that the negative effects of the latter could be mitigated by combining it with the former to culture niche cells which could be used to culture MSCs, ECFCs and HSCs in a more advanced bone marrow model. Further research should focus on the immunometabolic changes occurring while culturing these cells in Stem Span media. Furthermore, our findings suggest that when introducing different environments through the addition of substrates, different media compositions or external stimuli, the time point at which they are introduced should also be taken into consideration rather than the concentrations and quantities.

This project laid the foundation for the fabrication of an in vitro model capable of recapitulating the physiology of native bone marrow suitable to home functioning HSCs. Ultimately, recreating

the bone marrow environment will enable better HSC functionality while maintaining the stemness and pool of progenitors for longer.

5 Acknowledgements

This study was conducted at Regenerative Medicine Centre Utrecht, in the Levato Lab under the supervision of Riccardo Levato and Marisa de Oliveira Assunçao.

References

[1] A. Mendelson and P. S. Frenette, "Hematopoietic stem cell niche maintenance during homeostasis and regeneration," *Nat. Med.*, vol. 20, pp. 833–846, Aug. 2014.

[2] D. N. Tavakol, J. Chen, N. W. Chavkin, T. N. Tavakol, K. K. Hirschi, and G. Vunjak-Novakovic, "Lessons from biology: Engineering design considerations for modeling human hematopoiesis," 2021.

[3] J. Zheng, C. Song, and C. C. Zhang, "A new chapter: hematopoietic stem cells are direct players in immunity," *Cell Biosci.*, vol. 1, p. 33, Oct. 2011.

[4] L. Teofili, M. Martini, E. R. Nuzzolo, S. Capodimonti, M. G. Iachininoto, A. Cocomazzi, E. Fabiani, M. T. Voso, and L. M. Larocca, "Endothelial progenitor cell dysfunction in myelodysplastic syndromes: possible contribution of a defective vascular niche to myelodysplasia," *Neoplasia*, vol. 17, pp. 401–409, May 2015.

[5] K. S. Lim, B. J. Klotz, G. C. J. Lindberg, F. P. W. Melchels, G. J. Hooper, J. Malda, D. Gawlitta, and T. B. F. Woodfield, "Visible light Cross-Linking of gelatin hydrogels offers an enhanced cell microenvironment with improved light penetration depth," *Macromol. Biosci.*, vol. 19, p. e1900098, June 2019.

[6] N. He, L. Zhang, J. Cui, and Z. Li, "Bone marrow vascular niche: home for hematopoietic stem cells," *Bone Marrow Res.*, vol. 2014, p. 128436, Apr. 2014.

[7] P. Ramalingam, M. G. Poulos, and J. M. Butler, "Regulation of the hematopoietic stem cell lifecycle by the endothelial niche," *Curr. Opin. Hematol.*, vol. 24, pp. 289–299, July 2017.

[8] L. I. Zon, "Intrinsic and extrinsic control of haematopoietic stem-cell self-renewal," *Nature*, vol. 453, pp. 306–313, May 2008.

[9] S. W. Lane, D. A. Williams, and F. M. Watt, "Modulating the stem cell niche for tissue regeneration," *Nat. Biotechnol.*, vol. 32, pp. 795–803, Aug. 2014.

[10] P. A. Hall and F. M. Watt, "Stem cells: the generation and maintenance of cellular diversity," *Development*, vol. 106, pp. 619–633, Aug. 1989.

[11] F. M. Watt and W. T. S. Huck, "Role of the extracellular matrix in regulating stem cell fate," *Nat. Rev. Mol. Cell Biol.*, vol. 14, pp. 467–473, Aug. 2013.

[12] C. Lee-Thedieck and J. P. Spatz, "Biophysical regulation of hematopoietic stem cells," *Biomater Sci*, vol. 2, pp. 1548–1561, Nov. 2014.

[13] P. Zhang, C. Zhang, J. Li, J. Han, X. Liu, and H. Yang, "The physical microenvironment of hematopoietic stem cells and its emerging roles in engineering applications," *Stem Cell Res. Ther.*, vol. 10, p. 327, Nov. 2019.

[14] B. Antebi, L. A. Rodriguez, 2nd, K. P. Walker, 3rd, A. M. Asher, R. M. Kamucheka, L. Alvarado, A. Mohammadipoor, and L. C. Cancio, "Short-term physiological hypoxia potentiates the therapeutic function of mesenchymal stem cells," *Stem Cell Res. Ther.*, vol. 9, p. 265, Oct. 2018.

[15] J. A. Spencer, F. Ferraro, E. Roussakis, A. Klein, J. Wu, J. M. Runnels, W. Zaher, L. J. Mortensen, C. Alt, R. Turcotte, R. Yusuf, D. Côté, S. A. Vinogradov, D. T. Scadden, and C. P. Lin, "Direct measurement of local oxygen concentration in the bone marrow of live animals," *Nature*, vol. 508, pp. 269–273, Apr. 2014.

[16] D. Lucas, C. Scheiermann, A. Chow, Y. Kunisaki, I. Bruns, C. Barrick, L. Tessarollo, and P. S. Frenette, "Chemotherapy-induced bone marrow nerve injury impairs hematopoietic regeneration," *Nat. Med.*, vol. 19, pp. 695–703, June 2013.

[17] S. A. Patel and P. Rameshwar, "Stem cell transplantation for hematological malignancies: Prospects for personalized medicine and co-therapy with mesenchymal stem cells," *Curr. Pharmacogenomics Person. Med.*, vol. 9, pp. 229–239, Sept. 2011.

[18] D. E. Glaser, M. B. Curtis, P. A. Sariano, Z. A. Rollins, B. S. Shergill, A. Anand, A. M. Deely, V. S. Shirure, L. Anderson, J. M. Lowen, N. R. Ng, K. Weilbaecher, D. C. Link, and S. C. George, "Organ-on-a-chip model of vascularized human bone marrow niches," *Biomaterials*, vol. 280, p. 121245, Jan. 2022.

[19] D. Wu, Z. Wang, J. Li, Y. Song, M. E. M. Perez, Z. Wang, X. Cao, C. Cao, S. Maharjan, K. C. Anderson, D. Chauhan, and Y. S. Zhang, "A 3D-Bioprinted multiple myeloma model," *Adv. Healthc. Mater.*, vol. 11, p. e2100884, Apr. 2022.

[20] P. N. Bernal, P. Delrot, D. Loterie, Y. Li, J. Malda, C. Moser, and R. Levato, "Volumetric bioprinting of complex Living-Tissue constructs within seconds," *Adv. Mater.*, vol. 31, p. e1904209, Oct. 2019.

[21] P. N. Bernal, M. Bouwmeester, J. Madrid-Wolff, M. Falandt, S. Florczak, N. G. Rodriguez, Y. Li, G. Größbacher, R.-A. Samsom, M. van Wolferen, L. J. W. van der Laan, P. Delrot, D. Loterie, J. Malda, C. Moser, B. Spee, and R. Levato, "Volumetric bioprinting of organoids and optically tuned hydrogels to build Liver-Like metabolic biofactories," *Adv. Mater.*, vol. 34, p. e2110054, Apr. 2022.

[22] K. S. Lim, F. Abinzano, P. N. Bernal, A. Albillos Sanchez, P. Atienza-Roca, I. A. Otto, Q. C. Peiffer, M. Matsusaki, T. B. F. Woodfield, J. Malda, and R. Levato, "One-Step photoactivation of a Dual-Functionalized bioink as cell carrier and Cartilage-Binding glue for chondral regeneration," *Adv. Healthc. Mater.*, vol. 9, p. e1901792, Aug. 2020.

[23] B. G. Soliman, G. S. Major, P. Atienza-Roca, C. A. Murphy, A. Longoni, C. R. Alcala-Orozco, J. Rnjak-Kovacina, D. Gawlitta, T. B. F. Woodfield, and K. S. Lim, "Development and characterization of Gelatin-Norbornene bioink to understand the interplay between physical architecture and Micro-Capillary formation in biofabricated vascularized constructs," *Adv. Healthc. Mater.*, vol. 11, p. e2101873, Jan. 2022.

[24] B. J. Klotz, D. Gawlitta, A. J. W. P. Rosenberg, J. Malda, and F. P. W. Melchels, "Gelatin-Methacryloyl hydrogels: Towards Biofabrication-Based tissue repair," *Trends Biotechnol.*, vol. 34, pp. 394–407, May 2016.

[25] M. Sun, X. Sun, Z. Wang, S. Guo, G. Yu, and H. Yang, "Synthesis and properties of gelatin methacryloyl (GelMA) hydrogels and their recent applications in Load-Bearing tissue," *Polymers*, vol. 10, Nov. 2018.

[26] W. Hu, Z. Wang, Y. Xiao, S. Zhang, and J. Wang, "Advances in crosslinking strategies of biomedical hydrogels," *Biomater Sci*, vol. 7, pp. 843–855, Feb. 2019.

[27] F. P. W. Melchels, M. M. Blokzijl, R. Levato, Q. C. Peiffer, M. de Ruijter, W. E. Hennink, T. Vermonden, and J. Malda, "Hydrogel-based reinforcement of 3D bioprinted constructs," *Biofabrication*, vol. 8, p. 035004, July 2016.

[28] D. Loterie, P. Delrot, and C. Moser, "High-resolution tomographic volumetric additive manufacturing," *Nat. Commun.*, vol. 11, p. 852, Feb. 2020.

[29] D. E. Ciolacu, "Structure-Property relationships in Cellulose-Based hydrogels," in *Cellulose-Based Superabsorbent Hydrogels* (M. I. H. Mondal, ed.), pp. 65–95, Cham: Springer International Publishing, 2019.

[30] K. S. Lim, R. Levato, P. F. Costa, M. D. Castilho, C. R. Alcala-Orozco, K. M. Van Dorenmalen, F. P. Melchels, D. Gawlitta, G. J. Hooper, J. Malda, *et al.*, "Bio-resin for high resolution lithography-based biofabrication of complex cell-laden constructs," *Biofabrication*, vol. 10, no. 3, p. 034101, 2018.

[31] C. A. Schneider, W. S. Rasband, and K. W. Eliceiri, "NIH image to ImageJ: 25 years of image analysis," *Nat. Methods*, vol. 9, pp. 671–675, July 2012.

[32] E. Zudaire, L. Gambardella, C. Kurcz, and S. Vermeren, "A computational tool for quantitative analysis of vascular networks," *PLoS One*, vol. 6, p. e27385, Nov. 2011.

[33] P. N. Bernal, P. Delrot, D. Loterie, Y. Li, J. Malda, C. Moser, and R. Levato, "Biofabrication: Volumetric bioprinting of complex living [U+2010] tissue constructs within seconds (adv. mater. 42/2019)," *Adv. Mater.*, vol. 31, p. 1970302, Oct. 2019.

[34] A. A. Zahid, R. Augustine, Y. B. Dalvi, K. Reshma, R. Ahmed, S. Raza Ur Rehman, H. E. Marei, R. Alfkey, and A. Hasan, "Development of nitric oxide releasing visible light crosslinked gelatin methacrylate hydrogel for rapid closure of diabetic wounds," *Biomed. Pharmacother.*, vol. 140, p. 111747, Aug. 2021.

[35] W. Schuurman, P. A. Levett, M. W. Pot, P. R. van Weeren, W. J. A. Dhert, D. W. Hutmacher, F. P. W. Melchels, T. J. Klein, and J. Malda, "Gelatin-methacrylamide hydrogels as potential biomaterials for fabrication of tissue-engineered cartilage constructs," *Macromol. Biosci.*, vol. 13, pp. 551–561, May 2013.

[36] L. B. Poole, "The basics of thiols and cysteines in redox biology and chemistry," *Free Radic. Biol. Med.*, vol. 80, pp. 148–157, Mar. 2015.

[37] C. Chen, F. Loe, A. Blocki, Y. Peng, and M. Raghunath, "Applying macromolecular crowding to enhance extracellular matrix deposition and its remodeling in vitro for tissue engineering and cell-based therapies," *Adv. Drug Deliv. Rev.*, vol. 63, pp. 277–290, Apr. 2011.

[38] C. C. Zhang and H. A. Sadek, "Hypoxia and metabolic properties of hematopoietic stem cells," *Antioxid. Redox Signal.*, vol. 20, pp. 1891–1901, Apr. 2014.

[39] S. W. S. Leung and Y. Shi, "The glycolytic process in endothelial cells and its implications," *Acta Pharmacol. Sin.*, vol. 43, pp. 251–259, Feb. 2022.

[40] A. Zecchin, J. Kalucka, C. Dubois, and P. Carmeliet, "How endothelial cells adapt their metabolism to form vessels in tumors," *Front. Immunol.*, vol. 8, p. 1750, Dec. 2017.

[41] W. Xiao, W. M. Oldham, C. Priolo, A. K. Pandey, and J. Loscalzo, "Immunometabolic endothelial phenotypes: Integrating inflammation and glucose metabolism," *Circ. Res.*, vol. 129, pp. 9–29, June 2021.

6 Appendix

6.1 Quantification of VBP Print Resolution

Table I: VBP scoring system for print resolution

Scores	Description of print
0	No print observed
1	No shape fidelity
2	Shape, wrong size, no features visible
3	Shape, wrong size, large feature
4	Shape, wrong size, small and large feature
5	Shape, right size, no features
6	Shape, right size, large feature
7	Shape, right size, small and large feature
8	Shape, right size, small and large feature, higher resolution

Table II: Optimization for finding optimal parameters to volumetric bioprint with RuSPS

Lightdose (mJ cm−2)	Ru (mM)	SPS (mM)	Score
450	0.1	10	6
470	0.1	10	7
480	0.1	15	3
500	0.1	15	3
450	0.1	20	1
550	0.1	20	3

Table III: Resolution of VBP printed constructs embedded with different cell densities

Lightdose (mJ cm−2)	Cell density (Million/mL)	Ru (mM)	SPS (mM)	Score
470	2	0.1	10	6
470	6.25	0.1	10	7
470	6.25	0.1	10	7
475	6.25	0.1	10	7
465	6.25	0.1	10	8

Table IV: Quantification of the features of the VBP printed constructs

Lightdose (mJ cm−2)	Cell density (Million/mL)	Ru (mM)	SPS (mM)	Score
470	2	0.1	10	6
470	6.25	0.1	10	7
470	6.25	0.1	10	7
475	6.25	0.1	10	7
465	6.25	0.1	10	8

Table V: Quantification of the features of the VBP printed constructs

	No cells	6.25(M/mL) 470(mJcm-2)	6.25 (M/mL) 465(mJcm-2)
Large Feature (2mm)	2,496±0,46	1,4905±0,013	1,4365±0,028
Small Feature (1mm)	0,7115±0,032	0,3975±0,009	0,475±0,025

6.2 Optimization of post curing time

Table VI: Finding the optimal post curing time

Lightdose (mJ cm−2)	Ru (mM)	SPS (mM)	Post curing (min)	Score
470	0.1	10	1	6
470	0.1	10	3	6
470	0.1	10	4	7
470	0.1	10	5	7

6.3 Optimization for printing with lower gelMA content

Table VII: Finding the optimal post curing time

Lightdose (mJ cm−2)	Ru (mM)	SPS (mM)	Score
520	0.08	8	6
530	0.08	8	6
540	0.08	8	7
550	0.08	8	6
555	0.08	8	6
560	0.08	8	7
565	0.08	8	6